Environ. Sci. Technol. **1998**, *32,* 2383−2388

Surface Structures and Stability of Arsenic(III) on Goethite: Spectroscopic Evidence for Inner-Sphere Complexes

BRUCE A. MANNING,*,† SCOTT E. FENDORF,‡ AND SABINE GOLDBERG†

USDA-ARS U.S. Salinity Laboratory, 450 West Big Springs Road, Riverside, California, 92507, and Soil Science Division, University of Idaho, Moscow, Idaho 83844-2339

The adsorption and stability of arsenite [As(III)] on goethite (α-FeOOH) was investigated using a combination of standard batch techniques and X-ray absorption spectroscopy (XAS). The reactivity of As(III) with α-FeOOH at varying pH and As(III) concentration provided macroscopic evidence for strong complexation on the α-FeOOH surface. Extended X-ray absorption fine structure (EXAFS) spectroscopy gave an average As(III)−Fe interatomic distance of 3.378 ± 0.014 Å, which is indicative of bidentate binuclear bridging As(III) complexes on the α-FeOOH surface and which is similar to other oxyanions which adsorb on α-FeOOH by an inner-sphere mechanism. X-ray absorption near-edge structure (XANES) analysis indicated that the As(III)−α-FeOOH surface complex is stable toward heterogeneous oxidation to As(V), as determined by the energy position of the X-ray absorption edge. The structural information from EXAFS was included in the description of As(III) adsorption on the α-FeOOH surface using a surface complexation model (the constant capacitance model). These results suggest that As(III) surface complex formation on iron(III) oxides may play an important role in the environmental behavior of arsenic.

Introduction

Elevated levels of arsenic can be present in the environment as a result of mineral weathering and dissolution (*1*, *2*), geothermal activity (*3*, *4*), and numerous anthropogenic sources including mine wastes (*5*), coal fly ash (*6*), and arsenical pesticides (*7*, *8*). The most prevalent species of dissolved As in the environment are arsenate [As(V)] and arsenite [As(III)], and both species are known to exist in groundwater (*9*). The mobility of As in the environment depends on As(III)/As(V) speciation, as well as the mineralogy of the soil, sediment, or groundwater material. Adsorption reactions on mineral surfaces, especially iron and aluminum oxides, can retain dissolved As and are well-studied phenomena in the literature. Though several recent spectroscopic studies of As(V) complexes on iron oxide have been published (*10*−*14*), little is known about the adsorption mechanism of As(III) on mineral surfaces.

Iron oxides have been recognized as reactive materials that are largely responsible for the attenuation of As in soils (*15*−*17*), lacustrine sediments (*18*, *19*), and marine sediments (*20*−*22*). Adsorption of dissolved As on mineral surfaces regulates pore water As concentrations in soils and sediments (*18*, *23*). The iron(III) oxide surface has a high affinity for As(V) capable of forming inner-sphere bidentate, binuclear As(V)−Fe(III) complexes (*10*, *12*, *14*, *24*). The As(III) species also has a high affinity for the iron(III) oxide surface (*25*−*27*) with evidence from FTIR spectroscopy for an inner-sphere adsorption mechanism similar to As(V) (*28*). Inner-sphere complexes are defined as covalent linkages between the adsorbed ion and the reactive surface with no water of hydration between the adsorbed ion and the surface functional group (*29*).

The importance of As(III) adsorption on iron(III) oxides in soil, groundwater, and reactive chemical barriers containing zerovalent Fe warrants careful investigation of the chemical structure and stability of As(III) complexes on iron(III) oxide mineral surfaces. This information is vital for modeling the transport and surface complexation of As(III) in the environment. Therefore, the objectives of this study were (1) to investigate the chemical structure of As(III) surface complexes on a model iron(III) oxide (goethite, α-FeOOH) using EXAFS, (2) to determine the stability of As(III) toward oxidation to As(V) on the α-FeOOH surface using XANES, and (3) to use the structural information from EXAFS in a surface complexation model to describe As(III) adsorption as a function of pH. Our approach used a combination of standard, batch adsorption experiments to investigate the macroscopic behavior of As(III) adsorption and XAS for determining the local atomic environment and oxidation state of As adsorbed on the α-FeOOH surface.

Experimental Section

Synthesis of α-FeOOH. The α-FeOOH used in this study was synthesized by adjusting the pH of a 0.2 M $Fe(NO_3)_3$ solution to 11.0 with 0.2 M NaOH and storing the resulting suspension at 22 ± 1 °C for 2 days (*30*). After heating in a water bath at 90 °C for 16 h followed by repeated rinsing of the solids with deionized (DI) water, the solids were dried for 16 h at 70 °C and ground with a mortar and pestle to pass a 500 mm sieve. The specific surface area was determined by single-point Brunauer−Emmett−Teller (BET) N_2 adsorption using a Quantasorb Jr. flow through surface area analyzer (Quantachrome Corp.). The identity of the material was confirmed as α-FeOOH by X-ray diffraction analysis of random powder mounts using CuKα radiation.

As(III) and As(V) Adsorption on α-FeOOH. Arsenic(III) adsorption envelopes (adsorption vs pH) were produced as batch reactions in 40 mL polycarbonate centrifuge tubes. A stock solution containing 13.33 mM As(III) was prepared by dissolving 0.867 g of $NaAsO_2$ (Sigma) in 500 mL of DI water and diluted for experiments. Twenty milliliter volumes of 2.5 g L^{-1} α-FeOOH suspension containing 133 mM or 266 mM As(III) were reacted for 16 h. The suspension pH was adjusted from 3 to 11 using not more than 0.25 mL of 0.1 M NaOH or HCl. Previous work (26, *31*) indicated that 99% of As(III) was removed from solution by amorphous $Fe(OH)_3$ after 4 h. The tubes were centrifuged (12500*g*, 10 min), the supernatant pH was measured with a glass combination pH electrode, and supernatants were then filtered through 0.45 mm pore size Whatman cellulose nitrate membranes. In a parallel experiment, an adsorption envelope containing 266 mM As(V) (as $Na_2AsO_4 \cdot 7H_2O$) was produced using the same reaction conditions as As(III). The amount of As adsorbed was calculated as the difference between the initial and final As concentration in solutions.

* Corresponding author. Phone: (909) 369-4884; fax: (909) 342-4962; e-mail: bmanning@ussl.ars.usda.gov.
† USDA-ARS U.S. Salinity Laboratory.
‡ University of Idaho.

S0013-936X(98)00220-X CCC: $15.00
Published on Web 06/26/1998

Dissolved As(III) and As(V) species were determined directly using high-performance liquid chromatography (HPLC) coupled with detection by hydride generation atomic absorption spectrophotometry (HGAAS) (*32*). Separation of As(III) and As(V) was achieved using a 30 mM NaOH/1% methanol mobile phase and Dionex AS-11 IonPac anion-exchange column which was in line with continuous, flow-through HGAAS. The HGAAS application used a Varian VGA 76 hydride generator which mixed sample solutions with 6 M HCl and 0.16 M $NaBH_4$ reagents.

Preparation of Samples for EXAFS and XANES Analysis. EXAFS and XANES spectroscopies were used to investigate the geometry and stability of the As(III) surface complex on α-FeOOH. Arsenic(III) surface coverage (Γ, mol m^{-2}) was varied by reacting 0.5 g of α-FeOOH with 200 mL of 0.065, 0.133, 0.267, 0.533, or 1.33 mM As(III) in 0.001 M NaCl for 16 h at constant pH (7.2 ± 0.2) in 250 mL polycarbonate centrifuge bottles. In similar α-FeOOH suspensions containing 0.267 mM As(III) in 0.001 M NaCl, the suspension pH was varied between 6.5 and 8.6 with 0.1 M HCl or NaOH. After 16 h, the suspensions were centrifuged (5000*g*, 10 min) and aliquots of the supernatant were filtered and analyzed for As(III)/As(V) speciation. The α-FeOOH solids were collected on filter papers and rinsed with DI water. The DI water rinse solution leachate was also filtered and analyzed for As(III)/As(V) speciation. Moist filter papers containing As(III)-treated α-FeOOH pastes were transferred to airtight, glass vials and stored 3−5 days prior to EXAFS analyses.

For samples investigated by XANES analysis, we used the same preparation method as EXAFS samples. However, certain samples were prepared 16 days prior to XANES analyses and stored as either moist pastes or air-dried to determine the effects of a short aging period (16 days) and hydration status on the stability of surface-bound As(III). Certain As(V)-treated α-FeOOH samples were also prepared for comparison with As(III).

EXAFS and XANES Analysis. The EXAFS and XANES analyses were performed at the Stanford Synchrotron Radiation Laboratory (SSRL). The K-edge of arsenic (11867 eV) was examined on beamline 4-1 (an 8 pole wiggler) using a Si(220) monochromator. We used an energy range of −200−1000 eV from the K-edge to acquire the EXAFS spectra. Samples were mounted as wet pastes in a 3 × 5 × 40 mm slot cut in an acrylic plate and sealed with Kapton polymide film to prevent moisture loss from the hydrated paste while minimizing X-ray absorption. Absorbance of the incident X-rays was measured by the intensity of the fluorescent X-rays using a 13 element Ge semiconductor detector (*33*).

For XANES analysis, energy steps of 0.3 eV were used across the edge region (11 850−11 900 eV) and the energy range was limited to −200−300 eV around the K-edge. Arsenic metal foil was used to calibrate the energy position of XANES spectra. The inflection points in XANES spectra, as noted by the intensity maxima in the first-derivative curves, were used to determine the oxidation state of As; the first-derivative peak position for As(III) is well-separated from As(V) by about 4 eV (*34*). The As(III)−goethite complexes were compared to standard compounds of reagent grade sodium arsenite ($NaAsO_2$) and sodium arsenate ($Na_2HAsO_4 \cdot 7H_2O$).

The EXAFS spectra were analyzed using EXAFSPAK computer software (*35*). For each sample, the five individual scans were averaged and the background X-ray absorbance of the averaged spectrum was subtracted by fitting a linear polynomial equation through the preedge region. The EXAFS spectra were then normalized to unity using a Victoreen polynomial function. A spline function was used to account for the atomic absorption in the absence of backscattering contributions and was fit to the absorption envelope and subtracted from the spectra over the energy range 11 920−12 869 eV. This isolated function was then transformed from units of electron volts to inverse angstroms to produce the EXAFS function [$\chi(k)$] where k ($Å^{-1}$) is the photoelectron wave vector. The $\chi(k)$ function was then weighted by k^3 and truncated leaving a k-range (k-window) of 3.36−12.5 $Å^{-1}$ for further analysis.

TABLE 1. Input Parameters and Chemical Reactions Used To Describe As(III) Adsorption on Goethite (α-FeOOH) in FITEQL

α-FeOOH surface area,	45 $m^2\ g^{-1}$
surface site density [SOH]	5×10^{-4} mol L^{-1}

solution reactions	log *K*	eq
$H_3AsO_3^0 \rightleftarrows H^+ + H_2AsO_3^-$	−9.23 (*43*)	1
$H_2AsO_3^- \rightleftarrows H^+ + HAsO_3^{2-}$	−12.0	2

surface reactions	log *K*(int)[a]	eq
$SOH^b + H^+ \rightleftarrows SOH_2^+$	5.967	3
$SOH \rightleftarrows SO^- + H^+$	−10.60	4
$2SOH + H_3AsO_3^0 \rightleftarrows S_2HAsO_3^0 + 2H_2O$	9.220	5
$2SOH + H_3AsO_3^0 \rightleftarrows S_2AsO_3^- + 2H_2O + H^+$	0.511	6

[a] Intrinsic surface complexation constants [*K*(int)] were calculated as moles per liter where $K(\text{int}) = K\exp(-nF\Psi_o/RT)$, K is the equilibrium constant for the reaction, n is the stoichiometric coefficient, F is the Faraday (9.65×10^{-4} C mol^{-1}), Ψ_o is the surface potential (V), R is the gas constant, and T is the temperature (K). [b] SOH represents one reactive surface hydroxyl group bound to a surface metal ion S.

The k^3-weighted $\chi(k)$ function [$\chi(k)k^3$] in k-space ($Å^{-1}$) was Fourier transformed (FT) to produce the radial structure function (RSF) in R-space (Å). Major peaks in the RSF correspond to atomic shells around the As atom (e.g., As−O and As−Fe) that backscatter the outgoing photoelectron waves. The FT was then repeated and two major peaks in the RSF (corresponding to As−O and As−Fe shells) were chosen for further analysis. The As−O and As−Fe RSF peaks were isolated by selecting the R-window as the minimum amplitude points at low and high distance points around a peak resulting in As−O and As−Fe R-windows of 1.02−1.71 Å and 2.69−3.30 Å, respectively. The individual As−O and As−Fe R-windows and the composite As−O + As−Fe R-window (1.02−3.30 Å) were backtransformed to produce the Fourier-filtered (FF) EXAFS functions. In addition to the FF EXAFS spectra, the unfiltered EXAFS spectra were also used in the final parameter fitting process.

Fourier-filtered experimental EXAFS data were first fit with a theoretical EXAFS expression in which the number of coordinating atoms (N), their distance (R), and disorder (σ^2) were varied to give the best fit between filtered experimental and predicted spectra. An additional variable, the energy offset (E_0), was used in the first As−O shell fits (R-window = 1.02−1.71 Å). After the E_0 was obtained in the As−O shell, this parameter was fixed for the higher (R-window = 2.69−3.30 Å) As−Fe shell and composite shell (R-window = 1.02−3.30 Å). Phase and amplitude functions for the absorber and backscatterers were defined using the single scattering, curved wave FEFF model (*36*, *37*). After the individual peaks in the RSF were backtransformed and fit, the composite (As−O + As−Fe) FF EXAFS function was modeled using the same parameters with optimization of the N, R, and σ^2 parameters being performed again. Finally, the fitted parameters were used to model the unfiltered EXAFS function. Error estimates of the fitted parameters were $R \pm$ 0.02 Å, $N \pm$ 20%, and $\sigma^2 \pm$ 20−30%.

Surface Complexation Modeling. A surface complexation model (the constant capacitance model, CCM) was used to describe the As(III) adsorption envelope (adsorption vs pH) on α-FeOOH. In the present study, the reactions explained

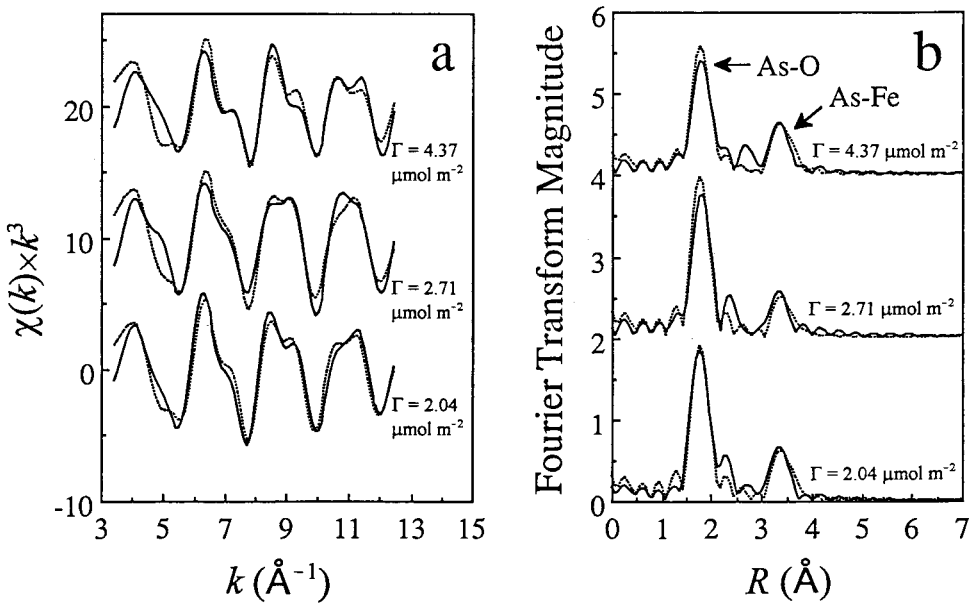

FIGURE 1. Fourier filtered EXAFS data for three As(III) surface coverages on goethite (α-FeOOH) at pH 7.2−7.4: (a) k^3-weighted $\chi(k)$ (EXAFS) functions and (b) their corresponding radial structure functions (RSF). Solid lines represent the filtered experimental EXAFS and RSF data and dotted lines are the fits derived from the theoretical EXAFS function in EXAFSPAK.

TABLE 2. EXAFS Equation Parameters Optimized Using EXAFSPAK for the Filtered EXAFS of the As(III)−Goethite Surface Complex

As(III) surface coverage (μmol m^{-2})	pH	As−O Shell			As−Fe Shell				
		N[a]	R (Å)	σ^2	N	R (Å)	σ^2	E_0	F
4.37	7.4	3.026	1.794	3.04×10^{-3}	2.440	3.379	6.39×10^{-3}	−2.443	91.9
2.71	7.4	3.048	1.789	1.75×10^{-3}	2.367	3.378	4.51×10^{-3}	−2.514	118
2.04	7.2	3.026	1.790	2.62×10^{-3}	2.571	3.401	5.86×10^{-3}	−2.627	66.6
1.87	6.4	3.120	1.791	2.99×10^{-3}	2.305	3.360	5.25×10^{-3}	−1.046	75.9
1.92	8.6	3.090	1.782	2.62×10^{-3}	2.447	3.373	7.05×10^{-3}	−2.536	64.6

[a] N = coordination number; R = interatomic distance; σ^2 = Debye Waller factor; E_0 = threshold E_0 shift in electron volts (used for both shells); F = goodness of fit parameter (sum of squares of differences between experimental and calculated curves).

in Table 1 were used to describe As(III) surface complex formation. The FITEQL computer program (*38*) was used to fit the set of surface complexation constants for eqs 3−6 in Table 1 to experimental adsorption data. The CCM has been used successfully in a prior study to describe As(III) and As(V) adsorption on clay minerals (*39*), and more detail on the application of FITEQL and the CCM can be found in previous papers (*39*−*42*). The most likely complex formed as determined by EXAFS analysis was used in the surface complexation reactions in the CCM.

Results and Discussion

EXAFS and XANES Analysis of As(III) on α-FeOOH. The Fourier-filtered $\chi(k)k^3$ data for the three As(III) surface coverages and their corresponding RSF data in R-space (Å) are shown in Figure 1. The parameters listed in Table 2 were derived by obtaining the best possible fits of the theoretical EXAFS expression to Fourier-filtered data (dotted lines, Figure 1a). Only slight differences were found in the final optimized values of N and R over the pH range 6.5−8.6 (data not shown) and As(III) surface coverages.

Fitting the theoretical EXAFS expression to experimental data revealed that the As−O first shell backscatterer peak at an average interatomic distance of 1.789 ± 0.004 Å was composed of an average of $N = 3.062 \pm 0.041$ O atoms (Table 2) which is in agreement with a previously published As(III)−O bond length of 1.78 ± 0.02 for arsenic trioxide (*43*). No significant differences in fitted As−O interatomic distances were found between individual samples. The second peak at 3.378 ± 0.014 Å results from the backscatterer contribution from $N = 2.426 \pm 0.099$ Fe atoms in the second atomic shell around the As absorber. An initial result of the EXAFS analysis is that the AsO_3 molecule appears to penetrate the octahedral coordination shell of Fe forming an inner-sphere complex.

It is important to note that R distances in all FT spectra (e.g., Figure 1b) correspond closely to the true crystallographic interatomic As−O and As−Fe distances because they have been oxygen-phase corrected. However, all interatomic distances (R) reported in Table 2 were derived from refinement to the EXAFS [$\chi(k)k^3$] data which were not phase corrected during Fourier filtering. Therefore, phase correction has been included in the final RSF representation in Figures 1b and 2b only as a visual aid and has no effect on the fitted R values in Table 2. The amount of displacement of R from true crystallographic As−Fe interatomic distance (ΔR) when phase correction is not used is approximately −0.3 Å (*44*−*46*).

Shoulders and smaller peaks in the filtered RSF plot (Figure 1b) in the R region between the two confirmed As−O and As−Fe peaks ($R \cong 2$−3 Å) were not considered in the final EXAFS data analysis. It is possible that minor backscatterer contributions indicated by smaller peaks in the RSF other than the two major As−O and As−Fe peaks were present. However, these were either mathematical artifacts or were below the sensitivity of our method. A final parameter optimization step involved fitting the theoretical EXAFS expression directly to the unfiltered, experimental EXAFS data (Figure 2). This resulted in slight refinements of the As−Fe R values of less than ±0.01 Å with negligible changes

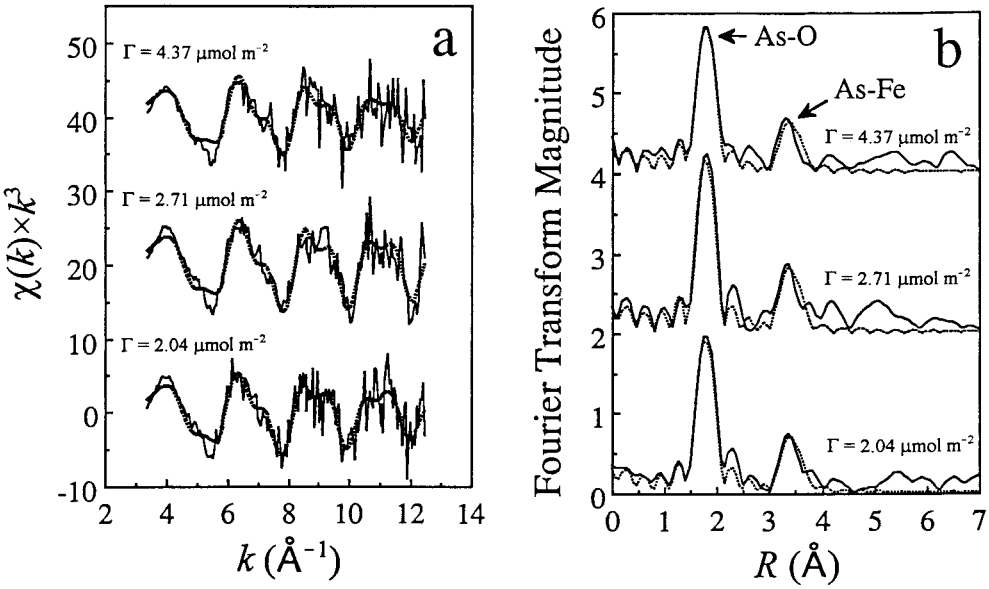

FIGURE 2. Unfiltered EXAFS data for three As(III) surface coverages on goethite (α-FeOOH) at pH 7.2−7.4: (a) k^3-weighted $\chi(k)$ (EXAFS) functions and (b) their corresponding radial structure functions (RSF). Solid lines represent the unfiltered experimental EXAFS and RSF data and dotted lines are the fits of the theoretical EXAFS function in EXAFSPAK using parameters in Table 2.

in other fitted parameters. The average *R* value for the As−Fe shell at 3.378 ± 0.014 Å is similar to values reported for other oxyanions. For example, the Se(IV)-Fe *R* values for Se(IV) adsorbed on α-FeOOH is 3.38 Å (*47*) whereas an *R* range of 3.34−3.36 was reported for Se(IV) on hydrous ferric oxide (HFO) (*48*).

Previous work using EXAFS spectroscopy to investigate As(V) adsorption on α-FeOOH has involved using multiple As−Fe shells to fit theoretical EXAFS function to experimental EXAFS data (*10*, *12*, *14*). The physical meaning of multiple As−Fe atomic shells involves postulating multiple bonding types, each bonding type resulting in a different As−Fe distance. For example, EXAFS data for As(V) adsorbed on α-FeOOH have been described using three As−Fe distances corresponding to a monodentate mononuclear complex [As(V)−Fe = 3.60 Å], a bidentate binuclear complex [As(V)−Fe = 3.24−3.26 Å], and a bidentate mononuclear complex [As(V)−Fe = 2.83−2.85 Å] (*14*).

On the basis of EXAFS analysis, the As(III) forms inner-sphere complexes on α-FeOOH, as noted by the As(III)−Fe shell distance of 3.378 Å. With an As(III)−Fe distance of 3.378 Å and the average fitted *N* value of 2.426 ± 0.099 Fe atoms, the most likely configuration of the As(III)−α-FeOOH surface species is a bidentate, binuclear bridging complex. Using a known crystallographic Fe(III)−O interatomic distance of 2.02 Å for goethite (*12*, *13*), and the As(III)−O and As(III)−Fe distances from EXAFS analysis, a structural diagram of the most likely geometry of the As(III)−α-FeOOH surface complex was constructed indicating H bonding at low pH and deprotonation on the surface complex at increased pH (Figure 3).

The formation of monodentate As(III) complexes was investigated by the inclusion of an additional shell of Fe atoms in the fit to the filtered Fe EXAFS function (data not shown). The Fe shell was included at an initial distance of 3.80 Å from the As atom, corresponding to a linear As−O−Fe bond configuration. After optimizing the second Fe shell *R* value, a final value of 3.57 Å provided the best fit to the experimental data, corresponding to a bent As−O−Fe configuration with an As−O−Fe bond angle 137° (tilt angle of 43°) (Figure 3). Though the addition of more adjustable parameters improved the fit as expected, the majority of backscattering is accounted for by the 3.38 Å Fe atomic shell. Therefore, the monodentate

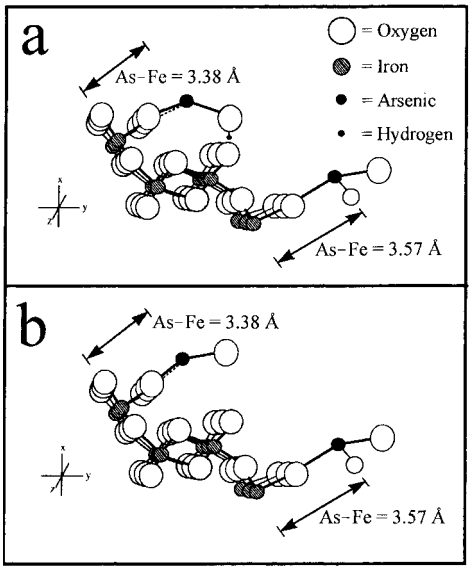

FIGURE 3. Structural diagram of bidentate binuclear and monodentate mononuclear As(III) surface complexes on the (110) plane of goethite (α-FeOOH) showing (a) the protonated bidentate surface species at 3.38 Å $S_2HAsO_3^0$ and (b) the deprotonated bidentate surface species ($S_2AsO_3^-$). Only the bidentate binuclear complex was used in surface complexation modeling.

As(III) complex was included in Figure 3 for illustration only and was not used in surface complexation modeling.

The XANES spectra of As(III)-treated α-FeOOH samples under hydrated and air-dried conditions were collected to test for possible As(III) oxidation to As(V) (Figure 4). The air-dried spectrum is shown off-set from the wet paste data by 0.07 fluorescence intensity units for visual inspection. Air-drying caused a small decrease in the fluorescence intensity maximum but caused no shift in the X-ray absorption edge position of the As(III)-treated α-FeOOH samples. All As(III)-treated α-FeOOH samples investigated showed energy positions indicative of As(III), suggesting that oxidation to As(V) on the α-FeOOH surface had not occurred. Additionally, first and final X-ray scans of samples were identical, indicating that oxidation of As(III) did not occur during exposure to the X-ray beam during XANES analysis.

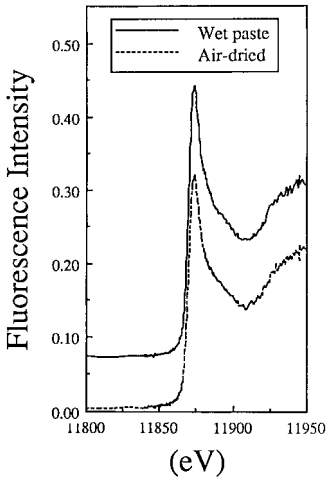

FIGURE 4. XANES spectra for As(III)-treated goethite (α-FeOOH) samples stored under hydrated (wet paste) and air-dried conditions.

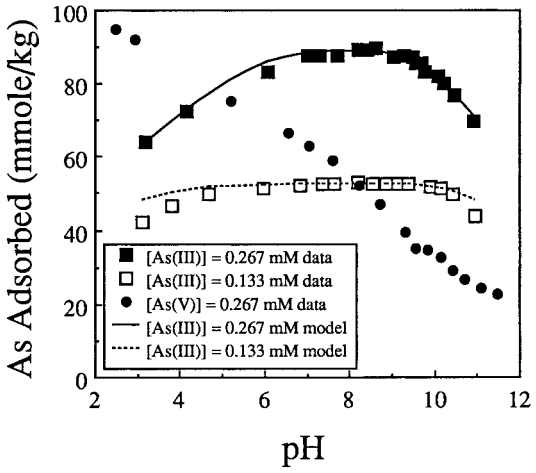

FIGURE 5. Experimental As(III) and As(V) adsorption envelopes on goethite (α-FeOOH) (points) with surface complexation model results for As(III) (lines) optimized in FITEQL.

Surface Complexation Modeling. The results of optimizing the CCM surface complexation constants in FITEQL are shown in Figure 5 and the final log *K*(int) values are listed in Table 1. The higher surface coverage data ($[As(III)]_o$ = 0.267 mM) were used for optimizing *K*(int) values followed by a prediction of the lower surface coverage data ($[As(III)]_o$ = 0.133 mM). The bidentate binuclear As(III) surface complex was used in the CCM description (eqs 5 and 6, Table 1) which resulted in an excellent agreement between experimental data and CCM output. Surface complexation models are capable of accommodating both monodentate and bidentate As surface complexes (*39*, *40*); however, the use of spectroscopy to confirm the As(III) attachment mechanism will improve the overall accuracy and predictive capability of the approach.

Also shown in Figure 5 is the As(V) adsorption envelope on α-FeOOH ($[As(V)]_o$ = 0.267 mM). The As(V) species displays adsorption behavior which is distinct from As(III) with an adsorption maximum at low pH. These data suggest that As(III) will be more strongly bound on iron oxide surfaces than As(V) at neutral to alkaline pH. The difference in macroscopic adsorption behavior between As(III) and As(V) may be partly related to differences in the structure of the As(III) and As(V) surface complexes. Apparently, As(III) forms a single bidentate binuclear As(III) surface structure, whereas As(V) forms at least two complexes (*12*, *14*).

The EXAFS results of this study showed that As(III) forms an inner-sphere, bidentate binuclear bridging complex on the surface of α-FeOOH with a pronounced As(III)−Fe second nearest neighbor bond distance of 3.38 Å. This As−Fe interatomic distance is similar to other oxyanions such as Se(IV). Both pH and As(III) surface coverage had only minor influences on the As−Fe interatomic distance (*R*) and coordination number (*N*). Evidence from XANES analysis suggested that As(III) remains stable on the α-FeOOH surface toward heterogeneous oxidation to As(V). The As(III) bidentate binuclear bridging complex was incorporated into a surface complexation model (CCM) and an excellent agreement was found between the model and As(III) adsorption data. This has implications for modeling the transport of oxyanion contaminants in the field because it will be possible to constrain the calibration of chemical models to describe the formation of known surface complexes.

Acknowledgments

The authors extend their gratitude to Drs. Glenn Waychunas and Paul Grossl for reviewing the manuscript, and to Dr. Graham George for assistance with the EXAFSPAK software and many helpful comments.

Literature Cited

(1) Tanaka, T. *Appl. Organomet. Chem.* **1988**, *2*, 283−295.
(2) Huang, Y.-C. In *Arsenic in the environment, part I: Cycling and characterization*; Nriago, J. O., Ed.; Wiley-Interscience: New York, 1988.
(3) Hering, J. G.; Chen, P.-Y.; Wilkie, J. A.; Elimelech, M.; Liang, S. *J. Am. Water Works Assoc.* **1996**, *88*, 155−167.
(4) Welch, A. H.; Lico, M. S.; Hughs, J. L. *Groundwater*, **1988**, *26*, 333−347.
(5) Bowell, R. J. *Appl. Geochem.* **1994**, *9*, 279−286.
(6) Davidson, R. L.; Natusch, D. S.; Wallace, J. R.; Evans, C. A. *Environ. Sci. Technol.* **1974**, *8*, 1107−1112.
(7) Peryea, F. J.; Creger, T. L. *Water Air Soil Pollut.* **1994**, *78*, 297−306.
(8) Mariner, P. E.; Holzmer, F. J.; Jackson, R. E.; Meinardus, H. W. *Environ Sci. Technol.* **1996**, *30*, 1645−1651.
(9) Korte, N. E.; Fernando, Q. *Crit. Rev. Environ. Control* **1991**, *21*, 1−39.
(10) Waychunas, G. A.; Fuller, C. C.; Rea, B. A.; Davis, J. A. *Geochim. Cosmochim. Acta* **1996**, *60*, 1765−1781.
(11) Waychunas, G. A.; Davis, J. A.; Fuller, C. C. *Geochim. Cosmochim. Acta* **1995**, *59*, 3655- 3661.
(12) Waychunas, G. A.; Rea, B. A.; Fuller, C. C.; Davis, J. A. *Geochim. Cosmochim. Acta* **1993**, *57*, 2251−2269.
(13) Manceau, A. *Geochim. Cosmochim. Acta* **1995**, *59*, 3647−3653.
(14) Fendorf, S.; Eick, M. J.; Grossl, P.; Sparks, D. L. *Environ. Sci. Technol.* **1997**, *31*, 315- 320.
(15) Elkhatib, E. A.; Bennett, O. L.; Wright, R. J. *Soil Sci. Soc. Am. J.* **1984**, *48*, 1025−1030.
(16) Livesey, N. T.; Huang, P. M. *Soil. Sci.* **1981**, *131*, 88−94.
(17) Fordham, A. W.; Norrish, K. *Aust. J. Soil Res.* **1979**, *17*, 307−316.
(18) Belzile, N.; Tessier, A. *Geochim. Cosmochim. Acta* **1990**, *54*, 103−109.
(19) Aggett, J.; Roberts, L. S. *Environ. Sci. Technol.* **1986**, *20*, 183−186.
(20) Sullivan, K. A.; Aller, R. C. *Geochim. Cosmochim. Acta* **1996**, *60*, 1465−1477.
(21) Belzile, N. *Geochim. Cosmochim. Acta* **1988**, *52*, 2293−2302.
(22) Peterson, M. L.; Carpenter, R. *Geochim. Cosmochim. Acta* **1986**, *50*, 353−369.
(23) Holm, T. R.; Anderson, M. A.; Stanforth, R. S.; Iverson, D. G. *Limnol. Oceanogr.* **1980**, *25*, 23−30.
(24) Lumsdon, D. G.; Evans, L. J. *J. Colloid Interface Sci.* **1994**, *164*, 119−125.
(25) Wilkie, J. A.; Hering, J. G. *Colloids and Surfaces A: Physicochemical and Engineering Aspects* **1996**, *107*, 97−110.
(26) Pierce, M. L.; Moore, C. B. *Water Res.* **1982**, *16*, 1247−1253.
(27) Raven, K. P.; Jain, A.; Loeppert, R. H. *Environ. Sci. Technol.* **1998**, *32*, 344−349.
(28) Sun, X.; Doner, H. E. *Soil Sci.* **1996**, *161*, 865−872.
(29) Sposito, G. *The Surface Chemistry of Soils.* Oxford University Press: Oxford, England, 1984.

(30) McLaughlin, J. R.; Ryden, J. C.; Syers, S. K. *J. Soil Sci.* **1981**, *32*, 365−377.
(31) Pierce, M. L.; Moore, C. B. *Environ. Sci. Technol.* **1980**, *14*, 214−216.
(32) Manning, B. A.; Martens, D. A. *Environ. Sci. Technol.* **1997**, *31*, 171−177.
(33) Cramer, S. P.; Tench, O.; Yocum, M.; George, G. N. *Nucl. Instr. Methods and Phys. A* **1988**, *266*, 586−591.
(34) Fendorf S.; McGeehan S. L. *Soil Sci. Soc. Am. J.* **1997**, (submitted).
(35) George, G. N., Pickering, I. J. *EXAFSPAK: A Suite of Computer Programs for Analysis of X-ray Absorption Spectra*. Stanford Synchrotron Radiation Laboratory, Stanford, CA, 1993.
(36) Mustre de Leon, J.,; Rehr, J. J.; Zabinsky, S. I.; Albers, R. C. *Phys. Rev. B* **1991**, *44*, 4146−4149.
(37) Rehr, J. J.; Mustre de Leon, J.; Zabinsky, S. I.; Albers, R. C. *J. Am. Chem. Soc.* **1991**, *113*, 5135−5140.
(38) Herbelin, A. L.; Westall, J. C. *FITEQL: A computer program for the determination of chemical equilibrium constants from experimental data*. Report 94-01, Oregon State University, Corvallis, OR, 1994.
(39) Manning, B. A.; Goldberg, S. *Environ. Sci. Technol.* **1997**, *31*, 2005−2011.
(40) Manning, B. A.; Goldberg, S. *Soil Sci. Soc. Am. J.* **1996**, *60*, 121−131.
(41) Goldberg, S.; Davis, J. A.; Hem, J. D. In *The Environmental Chemistry of Aluminum*; Sposito, G. Ed.; CRC Lewis Publishers: Boca Raton, Fl, **1996**.
(42) Dzombak, D. A.; Morel, F. M. M. *Surface Complexation Modeling, Hydrous Ferric oxide*. John Wiley & Sons: New York, 1990.
(43) Lide, D. R. (Ed.) *Handbook of Chemistry and Physics*, Chemical Rubber Company, Boca Raton, FL, 1991.
(44) Rehr, J. J.; Zabinsky, S. I.; Ankudinov, A.; Albers, R. C. *Physica B* **1995**, *209*, 23−26.
(45) McKale, A. G.; Veal, B. W.; Paulikas, A. P.; Chan, S. K.; Knapp, G. S. *J. Am. Chem. Soc.* **1988**, *110*, 3763−3768.
(46) Teo, B. K.; Lee, P. A. *J. Am. Chem. Soc.* **1979**, *101*, 2815−2822.
(47) Hayes, K. F.; Roe, A. L.; Brown, G. E.; Hodgson, K. O.; Leckie, J. O.; Parks, G. A. *Science* **1987**, *238*, 783−786.
(48) Manceau, A.; Charlet, L.; Boisset, M. C.; Didier, B.; Spadini, L. *Appl. Clay Sci.* **1992**, *7*, 201−223.

Received for review March 9, 1998. Revised manuscript received May 14, 1998. Accepted May 26, 1998.

ES9802201